SSCL-Preprint-93

SSCL-Preprint-93

Superconducting Super Collider Laboratory

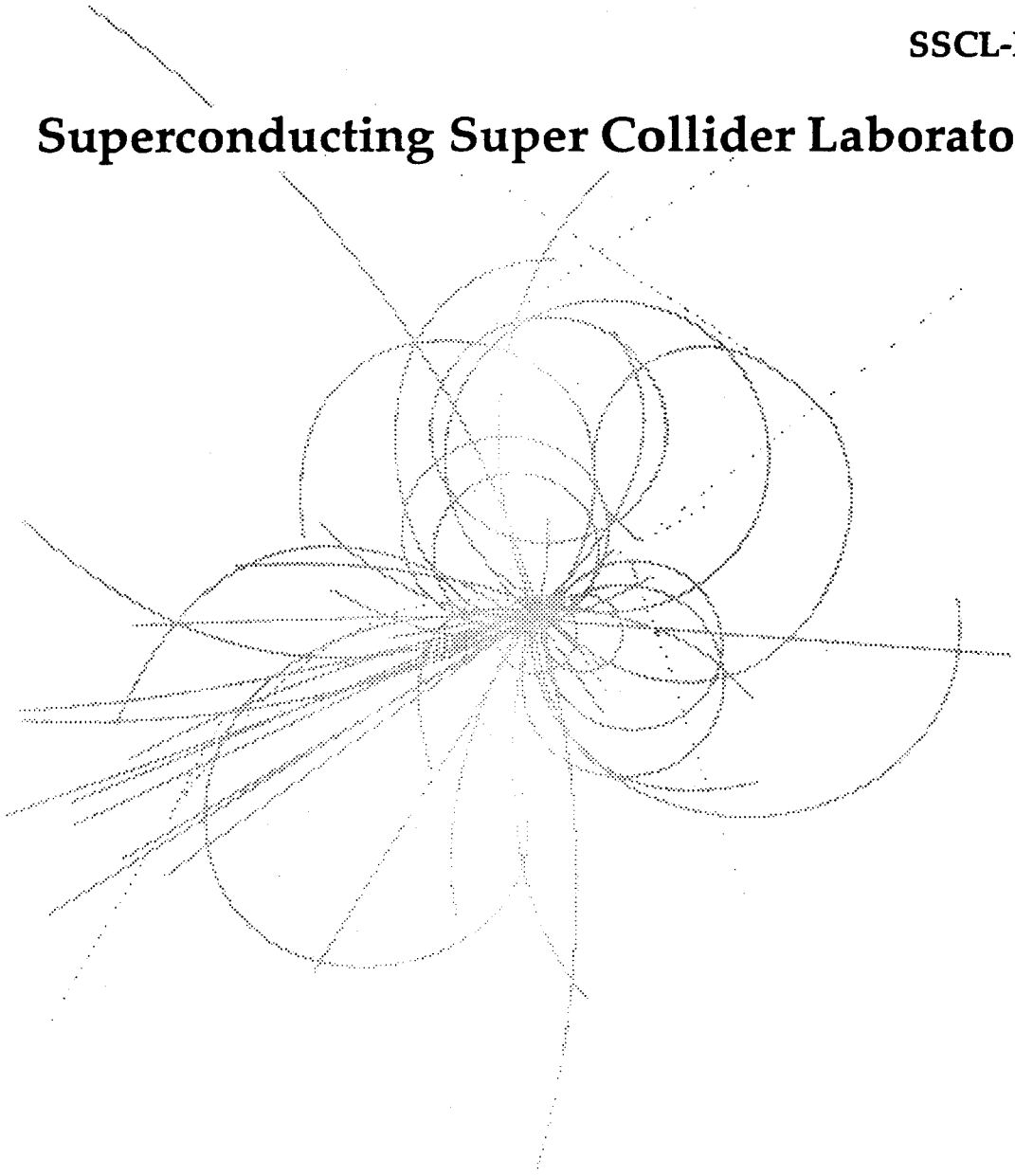

# Summaries of Performance of 40-mm and 50-mm Aperture SSC/BNL Collider Dipole Magnet Prototypes

C. Goodzeit and P. Radusewicz, et al.

March 1992

To be published in *Supercollider 4*

SSCL-Preprint-93

# Summaries of Performance of 40-mm and 50-mm Aperture SSC/BNL Collider Dipole Magnet Prototypes*

C. Goodzeit and P. Radusewicz, et al.

Superconducting Super Collider Laboratory†
2550 Beckleymeade Ave.
Dallas, TX 75237

March 1992

---

*Presented at the International Industrial Symposium on the Super Collider, New Orleans, March 4–6, 1992.

†Operated by the Universities Research Association, Inc., for the U.S. Department of Energy under Contract No. DE-AC35-89ER40486.

# CONSTRUCTION AND TEST RESULTS FROM 15 m-LONG, 50 mm APERTURE SSC COLLIDER DIPOLE MODELS*

M. Anerella, J. Cottingham, G. Ganetis, M. Garber, A. Ghosh, A. Greene, R. Gupta, A. Jain, S. Kahn, E. Kelly, G. Morgan, J. Muratore, A. Prodell, M. Rehak, E. P. Rohrer, W. Sampson, R. Shutt, R. Thomas, P. Thompson, P. Wanderer, E. Willen

Accelerator Development Department
Brookhaven National Laboratory,
Upton, New York 11973 USA

C. Goodzeit, P. Radusewicz

Superconducting Super Collider Laboratory
2550 Beckleymeade Ave.
Dallas, Texas 75237 USA

## ABSTRACT

Construction details, assembly data, coil stress and end force measurements are reported with quench data for the initial full-length SSC model dipoles with 50 mm aperture being built at BNL.

## INTRODUCTION

A series of six Collider Dipole model magnets are being assembled and tested at BNL. These magnets embody the design principles that have been employed in the previously tested series of 40 mm aperture magnets that have been built at BNL over the past few years in support of the SSCL program.[1] The major change in these magnets (in addition to the large aperture) is the use of wider cables for the inner and outer coils to provide an increased margin, greater than 10%, at operating field. Other basic design features that were used in the 40 mm magnets such as horizontally split yokes, internal ramp splices between the inner and outer coils and individually determined ends clamped in collars were retained. These magnets are instrumented with strain gauge collar packs to measure coil azimuthal stress and end force transducers to measure the force of the coil

*Work supported by the U.S.Department of Energy.

ends against their support. Voltage taps applied to the inner coil turns and at coil splices are installed in these magnets for quench origin determination. This paper discusses the design details and some test results for the first three magnets tested in this series. This includes mechanical assembly coil stress and end force histories, quench performance results and coil stress and end force measurements made during testing. Field quality and multipole measurements are discussed in a separate paper.[2]

## DESIGN

The magnets utilize a two-layer cosine Θ coil design with 50 mm aperture and 100 mm outer diameter. The details of the magnetic design of this magnet have been previously published.[3] The characteristics of the superconductor used in the three magnets discussed here are given in Table I. Table II lists the construction details for the three magnets. The two dimensional cross section of the cold mass is shown in Figure 1. The collars used in this cross-section have 4 mils of compensation. This means that the locations of the collar keyways are 6 mils closer to the midplane than those which would make the collar outside diameter perfectly circular. When tapered keys are inserted into the keyways and the clearance between the keys and keyway is 2 mils the vertical diameter of the keyed collar is 4 mils less than circular. This effect has been referred to as "anti-ovalization" and is now called compensation. This is to correct in part for the typical 10 mil vertical ovality created by deformation of the collars due to coil stress and insertion of the tapered keys.

| Cable Parameters, Mechanical | Inner Coil | Outer Coil |
|---|---|---|
| Filament diameter, $\mu$ | 6.0 | 6.0 |
| Strand diameter, mm | 0.808 | 0.648 |
| Number of strands | 30 | 36 |
| Bare cable width, mm | 12.34 | 11.68 |
| Bare cable mid-thickness, mm | 1.458 | 1.156 |
| Keystone (max/min) thickness, mm | 0.262 | 0.206 |

**Strand Properties Electrical**

| Magnet | Coil | Mfg. | Cu:SC | $J_c$ @ 5.6 T and 4.2 K | $J_c$ @ 7.0 T and 4.2 K |
|---|---|---|---|---|---|
| DCA207 | Inner-upper | IGC | 1.55 | 2716 | 1811 |
| | Inner-lower | IGC | 1.54 | 2661 | 1787 |
| | Outer-upper | IGC | 1.75 | 2397 | 1645 |
| | Outer-lower | IGC | 1.75 | 2397 | 1645 |
| DCA208 | Inner-upper | IGC | 1.34 | 2571 | 1732 |
| | Inner-lower | IGC | 1.34 | 2571 | 1732 |
| | Outer-upper | Oxford | 1.79 | 2638 | 1756 |
| | Outer-lower | Oxford | 1.76 | 2614 | 1740 |
| DCA209 | Inner-upper | Oxford | 1.5 | 2700 | 1835 |
| | Inner-lower | Oxford | 1.5 | 2700 | 1835 |
| | Outer-upper | Oxford | 1.83 | 2665 | 1771 |
| | Outer-lower | Oxford | 1.79 | 2629 | 1750 |

**Table I.**

| | |
|---|---|
| 1. | W6733 coil design. |
| 2. | Cable insulation: 48% overlap wrap of 25 $\mu$m Kapton type H film covered with a butt wrap of Hexcel F185 epoxy impregnated adhesive. |
| 3. | Solder filled internal ramp splice epoxy bonded to adjacent turn. |
| 4. | Collar design: 4 mil vertical OD compensation (reduction) |
| 5. | Collars spot welded, tapered (3° per side), alternating L/R pairs. Material: 21-6-9 stainless steel, strain hardened to 90,000 psi yield strength. |
| 6. | Collar packs: 6-inches long assembled on brass tubes and adjusted to length with variable brass shims in center of pack. |
| 7. | Outer coil scuff guard: brass, 15 mil. |
| 8. | Coil shims: brass, mechanically seated at collar pack ends. |
| 9. | Monolithic type (emulating a one-piece half-yoke) horizontally split. |
| 10. | Cross flow cooling. |
| 11. | Epoxy bonded stainless steel yoke modules at lead and return ends. |
| 12. | One piece, 1.5 inch (37 mm) stainless steel end plates welded to helium containment shell. |
| 13. | Helium containment shell extension with access ports for instrumentation mounted at lead and return ends, closure with dished heads. |
| 14. | Preloaded bullet type end force strain gauge transducers at both ends. |

**Table II.** Construction features of 17 m, 50 mm magnets DCA207-209.

The collared coils are installed into the yoke with a horizontal split line and nominal line to line fit between collar outside diameter and yoke inner diameter. The yoke is made up of individually assembled blocks that are stacked without gaps between them. Spacer laminations between the yoke blocks have slots which together with flow directional plugs on the collar and in the end plate bypass holes, provide the directed cross flow of helium for increased cooling in the annulus between the beam tube and inner coil. This is referred to as "cross flow cooling".[4] The yoke halves are prevented from lateral displacement by means of alignment keys at the horizontal split line.

Two .197 in. thick type 304 stainless steel shell halves are welded around the yoke at each side of the horizontal split line, separated from one another by stainless steel alignment rails, so that a total of four longitudinal welds are made for each magnet. During welding, closure of the yoke split line is verified by feeler gauge measurements through access ports in the alignment rails, which are later welded closed. At each end of the magnet, a 1.5 in. thick circular end plate is welded directly to the shell ends.

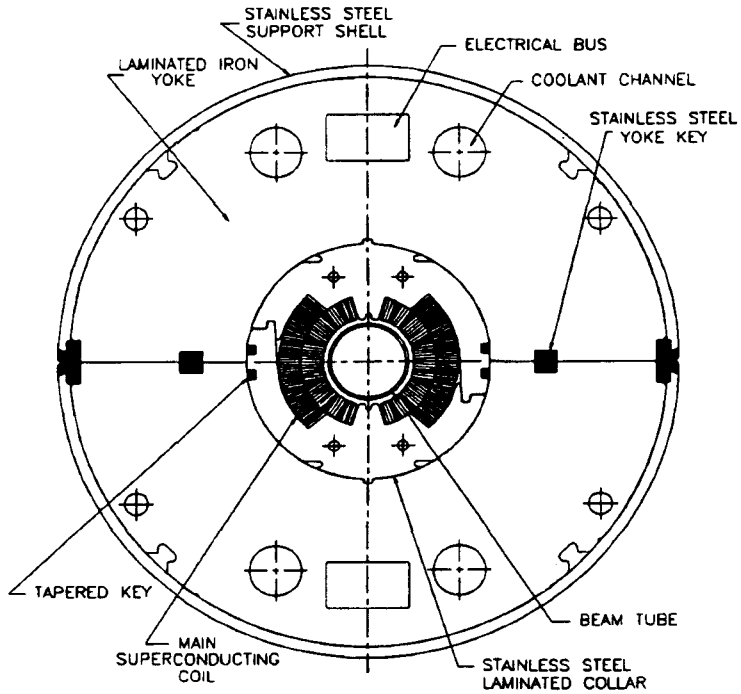


**Figure 1.** Cold mass cross section.

Figure 2 is a diagram of the construction of the cold mass at the lead end. The construction at the return end is similar. Coil end axial restraint is provided at each end by four instrumented set screws installed into threaded holes in the end plates. They are loaded against stainless steel pressure plates mounted to the coil ends.

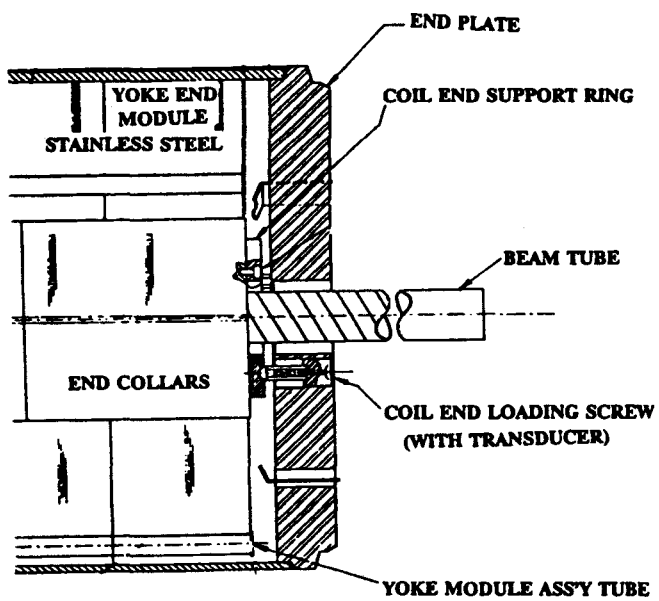


**Figure 2.** Return end.

The magnet cold mass is installed into a cryostat with multi-layer insulation and both a 4 K and 20 K heat shield. The magnet is supported at five locations with "folded post" type supports which minimize heat leaks. DCA207 utilized a BNL design cable bus; DCA208 and subsequent magnets feature an MIT design cable bus.

## COIL FABRICATION EXPERIENCE

All coils were cured at pressures higher than 7 kpsi due to the consistent use of oversized cable. Coils were molded to target sizes which would result in molding pressures of 7 kpsi when nominal size cable is used. The measured sizes of the molded coils, referenced to a standard of the design size, are given in Table III.

| Magnet | Coil | Azimuthal Size[1] (+mils) | Std. Dev./Max. Dev. (mils) |
|---|---|---|---|
| | | INNER COILS | |
| DCA207 | DCAI2001 | -0.5 | 1.4/4/5 |
| | DCAI2002 | -0.4 | 1.3/3.75 |
| DCA208 | DCAI2003 | -0.5 | 1.0/3.75 |
| | DCAI2004 | -2.4 | 1.3/4.75 |
| DCA209 | DCAI2005 | -0.8 | 0.9/3.5 |
| | DCAI2006 | -1.3 | 1.0/4.25 |
| | | OUTER COILS | |
| DCA207 | DCAO2001 | 8.3 | 1.5/5.25 |
| | DCAO2002 | 8.2 | 1.3/4.75 |
| DCA208 | DCAO2003 | 9.0 | 1.3/3.25 |
| | DCAO2004 | 8.1 | 0.8/3.0 |
| DCA209 | DCAO2005 | 9.1 | 1.0/4.0 |
| | DCAO2006 | 8.3 | 1.0/3.25 |

**[1] As compared to the magnetic design coil size, with coil measured while under the design compressive stress.**

**Table III.** 15 m SSC Coil Size Data.

## MECHANICAL BEHAVIOR

### Collaring and Assembly History

Assembly shim thicknesses were chosen in each case to provide the desired azimuthal coil stress after collar assembly. The inner coils used assembly shims larger than design by 15 mils; the outer coils used shims which matched the design value within 2 mils. (The relationship between measured coil size and required assembly shim thickness is not fully understood and shall be studied in the near future.)

The coils were mounted in collars and placed in the collaring press which applies both vertical and horizontal pressure to the collars to make use of the "tapered key"

method to collar these coils. The full-hard bronze keys have a three degree taper which when inserted into the keyways applies tension to the collars. This occurs at the end of the keying process and results in significantly less loss in coil stress when the hydraulic pressure is removed than if the tapered keys were not used. The inner coil stresses show an initial loss amounting to about 10% in the first hour. The rate of relaxation decreases significantly with time.

After collaring, (and when the coil stress relaxation has stabilized) the fit of the collar into the yoke was verified by measuring the deflection of the collars containing the compressed coils. Measurements were taken at 6-inch intervals along the length of the straight section of the coils and at one inch intervals at both the lead and return ends. These measurements record the vertical and horizontal dimensions. The fit of the collared coil in the yoke is inferred from these measurements using the measured inside diameter of the yoke laminations. The interference or gap for the three magnets as determined by this method is shown in Figure 3. The average coil stress for each magnet is indicated along the X-axis. It is seen that although there is some variation of the stress in each magnet the vertical yoke diametral interference is close to 7 mils in each case and that there is virtually a line to line fit of the collared coil into the yoke along the horizontal midplane.

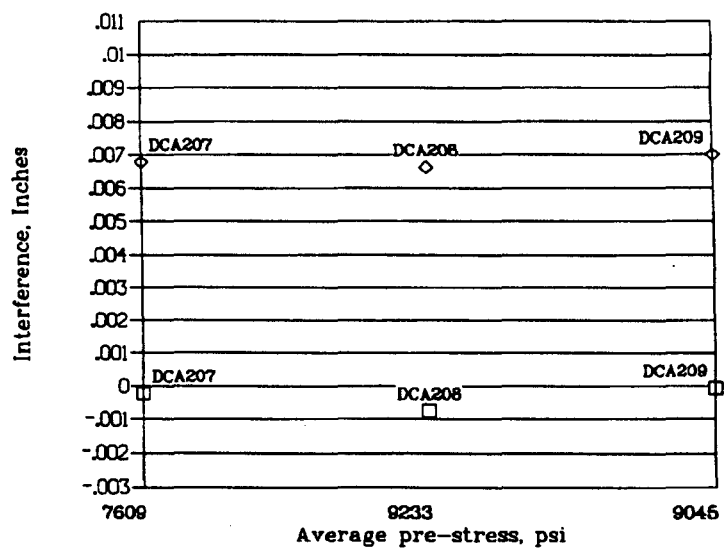


**Figure 3.** BNL ASST Magnets. Average collar-yoke interference in the magnet straight section (5.340" yoke I.D.). The vertical interference is indicated by ◇, the horizontal by □.

Coil Stress and End Forces

The coil stress histories and end force variation will be examined as follows:

- During the assembly steps up to test.
- Cool down and warm up effects.
- Coil Stress and End Force Effects in Testing.

In the discussion of the above effects, data from the assembly and testing of DCA209 will be used. DCA207 and DCA208 had similar behavior.

a. Coil Stress and End Force History

The stress history of the ambient temperature polar stress for the average inner and outer coil stresses is shown in Figure 4. Starting with the data that was taken a day after collaring, there is a steady relaxation of coil stress up to the time that the shell was welded. At the time the shell is welded there is an increase in stress as the coils are compressed by the tensile force induced in the shell by the welding process. The yoke horizontal midplane gap was measured to close after the root pass of shell welding for all three magnets. The rate of stress relaxation increases again at the higher stress levels after shell welding. The relaxation continues at a low rate and the stresses measured approximately 80 days after the shell welding and the magnet has completed testing show that the inner coil stress has dropped from 11,000 psi to 9800 psi and the outer coil stress has decreased from 9800 psi to 8800 psi.

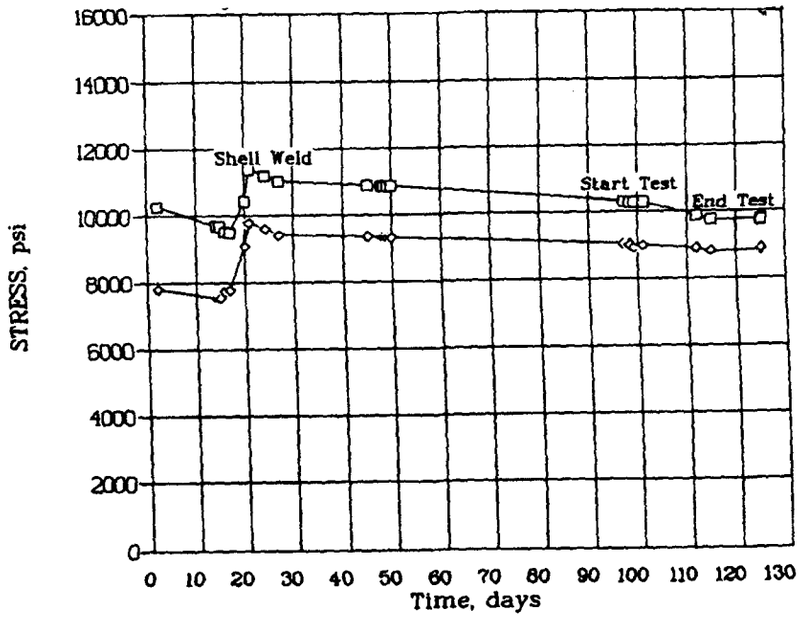


**Figure 4.** Magnet DCA209, Coil Stress at Ambient Temperature. The inner layer is indicated by □, the outer by ◇.

The end force history during the same period is somewhat more complicated and is shown in Figure 5 . The initial setting of the load screws that support the ends of the inner and outer coils is about 4000 lbs. per end. In order to complete the assembly of the cold mass a 7/16 inch wall cylinder is welded onto the end plate as shown in Figure 6. The purpose of this extension is to provide adequate space for the instrumentation boards and connections that are used in these model magnets. During this welding process the end force increased by about 10,000 lbs. on the lead end of the coil and by 6000 lbs. on the return end of the coil. This was believed to be caused by warpage of the end plate during the welding process. Referring to Figure 5 again, it is seen that the end force stays about the same until installation in the test stand where there is about a 1500 - 2000 lb. decrease. However, after the magnet had completed testing the end force at both the lead and return ends had increased to the 15000-20000 lb. range. This behavior was caused by a tendency of the end force to increase during testing. Figure 7 shows the end force for magnet DCA209 as a function of time throughout the first cold test cycle. Short arrows on the plot indicate excitations greater than 1000 A and long arrows represent excitation

whereby the magnet was quenched. From the plot one observes that with each magnet excitation there is a corresponding increase in the end force. A possible explanation for this is due to a retention of a portion of the axial Lorentz force produced during magnet excitation at the coil ends. In this case, the Lorentz forces expand the coil axially. Following excitation, the friction between the collars and the yoke laminations may prevent the collared coil assembly from returning to its original position and therefore increase the end load.

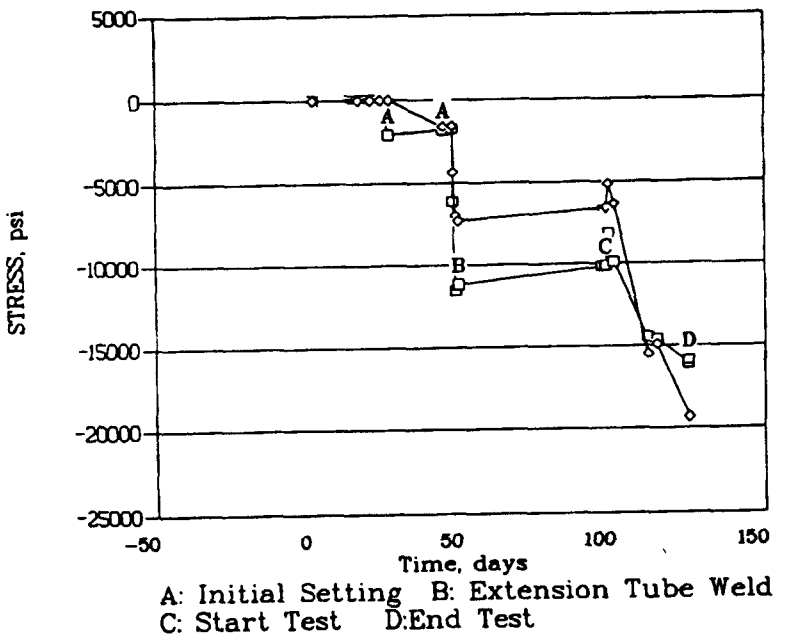


**Figure 5.** Magnet DCA209, End Force at Ambient Temperature. A: Initial Setting; B: Extension Tube Weld; C: Start Test; D: End Test. The lead end is indicated by □, the return end by ◇.

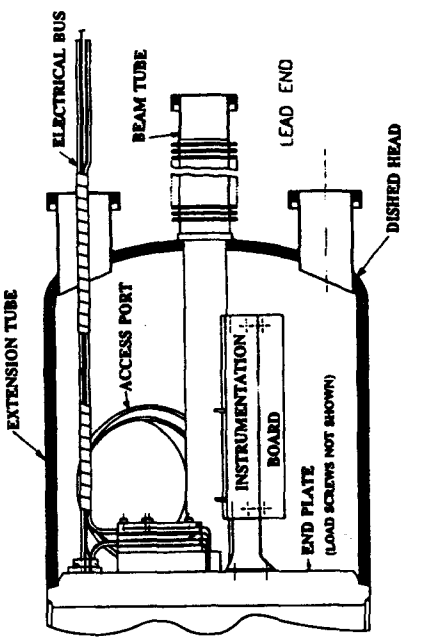


**Figure 6.** Lead end extension.

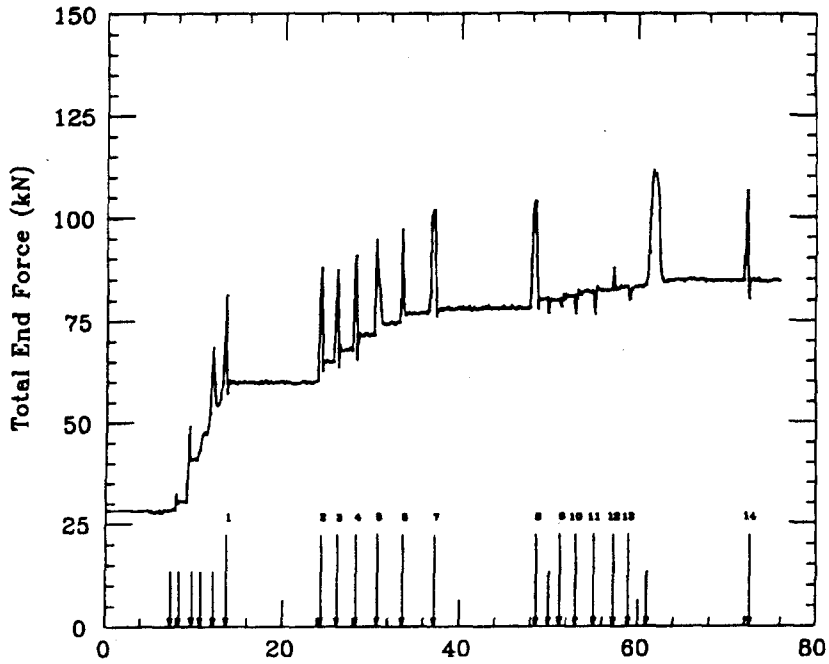


**Figure 7.** Magnet DCA209 1st Test Cycle Return End Force vs. time (hours).

b. Cool down and warm up effects

Table IV presents a summary of the changes in coils stress and end forces for the three magnets tested from the start to the completion of testing. There is some consistency in the amount of stress loss in the inner and outer coils when cooled from ambient to operating temperature. The coils typically loose about 4000 psi. The end forces are not as consistent from ambient to operating temperature. In some cases there is a small increase, in others a small decease. Characteristically it appears that they remain substantially the same through cool down. In most cases the end forces increase during testing as mentioned above; however, the return end force for DCA207 did not show this effect.

c. Coil stress and end force during magnet excitation

Data from the testing of DCA209 will be used to illustrate the effect of magnet excitation on the behavior of the coil stress and end forces. The variation of inner coil stress with current is shown in Figure 8. The polar stress indicated by the gauges in each quadrant is plotted as a function of magnet current squared. The serial number of the gauges is shown in the legend. Note that the stress deceases somewhat quadratically with current to about the operating point at 6600 A. At that time the poles of the coils are still under compression. This run was made under sub-cooled conditions so that the magnet could be powered above 8000 A. It is seen that as the current rises above 7000 A, the slope of the curves start to flatten out indicating that the coils are becoming unloaded at the poles. This gives a good method of verifying the cold calibration of the gauges since the flat part of the curves indicate zero polar stress. The offset shown of several hundred psi is the error in the compensating gauges resistance tracking with the active gauges. Thus one can correct these curves to indicate zero stress at above ~7500 A. Note that these magnets are capable of running well above the point where the poles of the inner

coils have become unloaded without quenching.

| | DCA207 | DCA208 | DCA209 |
|---|---|---|---|
| Inner coil stress (psi): | | | |
| 1. Before cooldown | 11292 | 9370 | 10295 |
| 2. After cooldown | 6617 | 5317 | 6428 |
| 3. Change | 4675 | 4053 | 3867 |
| 4. Percent loss | 41.4% | 43.3% | 37.6% |
| 5. Warm, after test | 10307 | 8919 | 9742 |
| 6. Delta for test | -985 | -451 | -553 |
| 7. Percent change for test | -8.7% | -4.8% | -5.4% |
| Outer coil stress (psi): | | | |
| 1. Before cooldown | 7399 | 8117 | 8994 |
| 2. After cooldown | 3988 | 3596 | 4778 |
| 3. Change | 3411 | 4521 | 4216 |
| 4. Percent loss | 46.1% | 55.7% | 46.9% |
| 5. Warm, after test | 7045 | 7851 | 8898 |
| 6. Delta for test | -354 | -266 | -96 |
| 7. Percent change for test | -4.8% | -3.3% | -1.1% |
| Lead end force (pounds): | | | |
| 1. Before cooldown | 14493 | 9975 | 9901 |
| 2. After cooldown | 10685 | 11457 | 11722 |
| 3. Change | 3808 | -1482 | -1821 |
| 4. Percent increase | -26.3% | 14.9% | 18.4% |
| 5. Warm, after test | 16652 | 14410 | 15868 |
| 6. Delta for test | 2159 | 4435 | 5967 |
| 7. Percent change for test | 14.9% | 44.5% | 60.3% |
| Return end force (pounds): | | | |
| 1. Before cooldown | 15595 | 11375 | 6347 |
| 2. After cooldown | 14262 | 11415 | 7090 |
| 3. Change | 1333 | -40 | -743 |
| 4. Percent increase | -8.5% | .4% | 11.7% |
| 5. Warm, after test | 13370 | 17214 | 19356 |
| 6. Change for test | -2225 | 5839 | 13009 |
| 7. Percent change for test | -14.3% | 51.3% | 205.0% |

**Table IV.** Summary of Stress and End Forces from Magnet Tests.

The behavior of the outer coils is somewhat different as shown in Figure 9 in which the outer coil quadrant stresses are plotted as a function of current squared. The Lorentz forces have relatively little effect on these coils and the stress only decreases a small amount with current. However, there is an interesting effect here. The curves of coil stress vs. current squared seem to show a dual slope. Initially the average slope for the gauges is $-7.07 \times 10^{-5}$ psi/A$^2$. However at ~4500 A, the slope becomes $-2.86 \times 10^{-5}$ psi/A$^2$. The interpretation is that there is a slight gap between the collars and the yoke near the mid plane. When the magnet is energized a horizontal component of the Lorentz force is produced which tends to increase the horizontal deflection of the collars. However, as soon as the collars contact the yoke, the bending stiffness of the yoke decreases the amount of horizontal deflection with force (and resulting stress decrease).

Thus, the slope of the curves become less. In this case, we assume that the collared coil is firmly supported by the yoke at 4500 A ($2 \times 10^7$ $A^2$), and above.

The change in end force with excitation is shown in Figure 10 in which the total end force at the lead and return end are plotted as a function of amperes squared. It is seen that these curves are quite linear and that the total end force change up to 8400 A is about 10,000 lbs. at the lead end and 6000 lbs. at the return end.

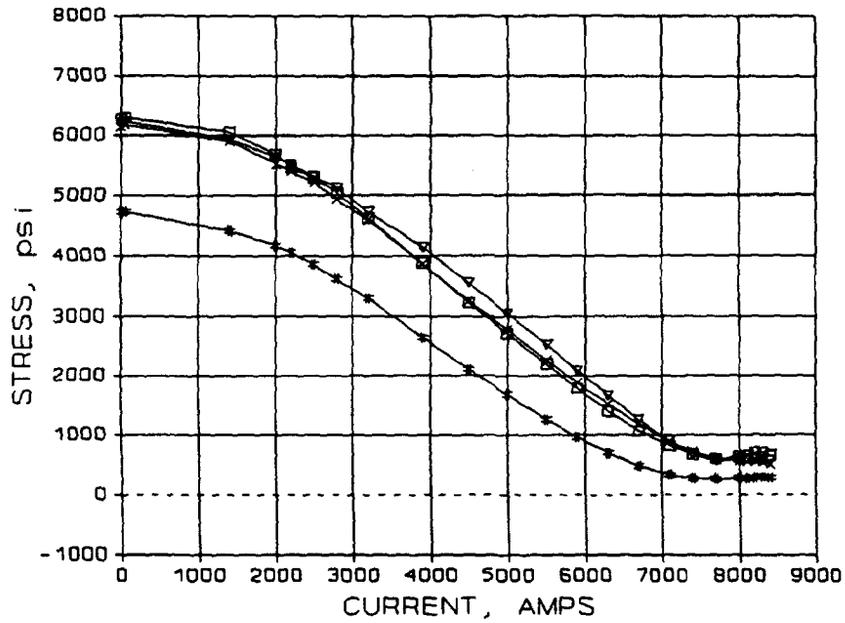


**Figure 8.** Magnet DCA209, inner coil stress (3.5 K) vs. I.

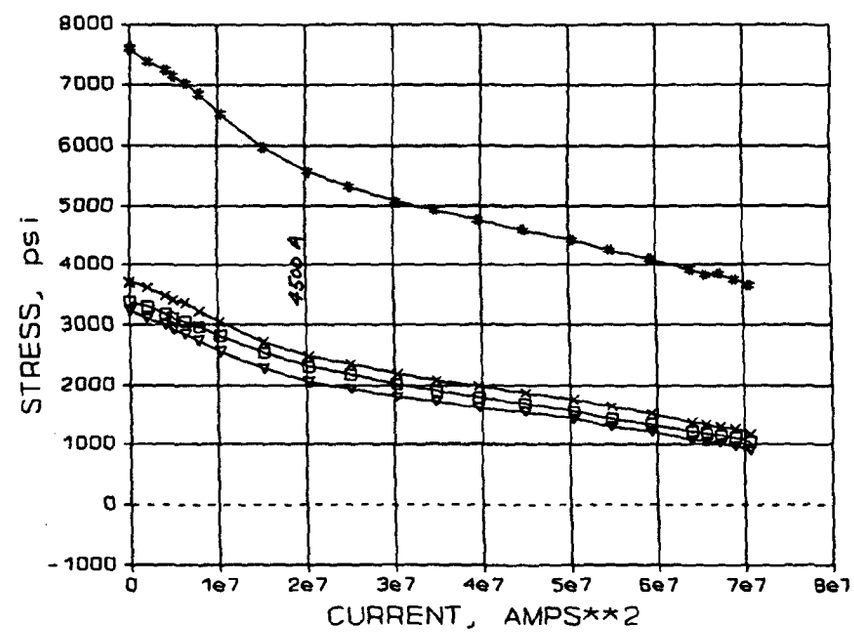


**Figure 9.** Magnet DCA209, Outer coil stress (3.5 K) versus $I^2$.

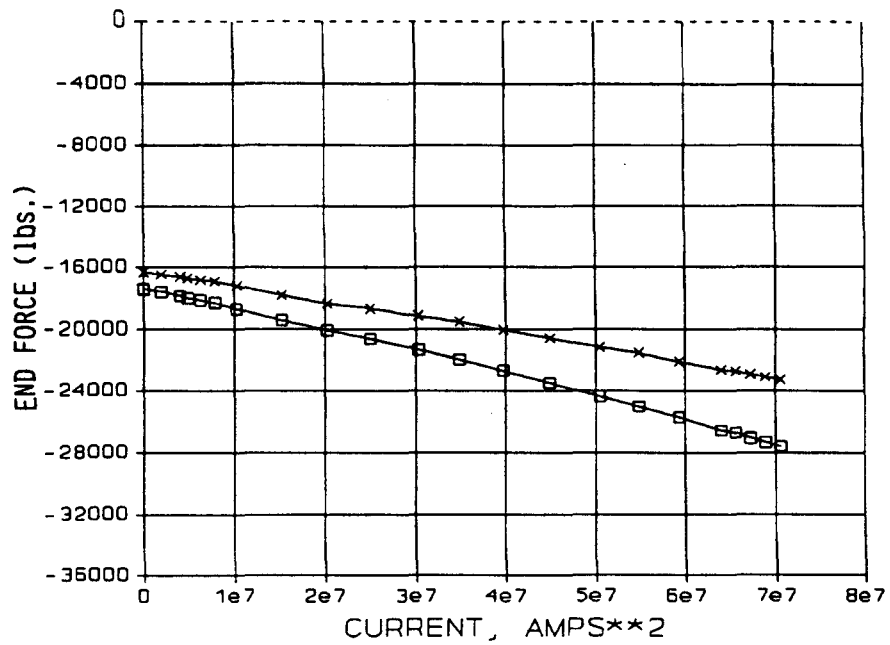


**Figure 10.** Magnet DCA209 lead end force (□) and return end force (X) vs. $I^2$ (3.5 K).

## QUENCH ANALYSIS

The quench test procedure for all three magnets consisted of ramping up the magnet current at a specified rate until a quench was generated, and performing this until the quench currents achieved had reached a four-quench plateau, within an allowable range of 30 A, and the quench origins were at locations that implied that they were conductor-limited. For the first quench at each testing temperature, a strain gauge run to quench, where the ramp was stopped at specific current steps to take strain gauge measurements on the way to quench, was used instead of a continuous ramp. In addition, at the end of each set of plateau quenches, strain gauge measurements were made at current steps almost up to quench plateau current and then on the way down again. Then, after a warm-up to room temperature and re-cooling (thermal cycle), a quench plateau was again established at 4.35 K. In the case of DSA207 and DSA209, quenching was also performed at the lower temperatures of 3.85 K and 3.5 K, where the central field is about 8.1 T and 8.5 T, respectively. The quenching at lower temperatures is done to test the limits of a magnet's mechanical performance under the stress of the higher magnetic fields possible at the lower temperatures. DCA208 was not tested under these conditions.

Figure 11 shows the quench history for the magnets tested. For brevity, the plot shows only the quenching at 4.35 K and does not exhibit quenches done at lower temperatures or those done at various ramp rates to study ramp-dependent effects. These results will be discussed later. All three magnets exhibited only minor training as they went quickly to plateaus which were close to values predicted from measurements of short sample cable. Small variations about the mean plateau quench current are attributed to cryogenic temperature fluctuations. All the plateau quenches were located in a straight section of a pole turn (turn 19) of an inner coil; this is expected for conductor-limited quenches, since these are the regions of highest magnetic field where the critical field can be expected to be reached first. It also should be noted that none of the magnets experienced quenches in the outer coils under any of the conditions imposed during the different testing regimes. As can be seen from the plot, DSA207 had two training

quenches at 7358 A and 7307 A, both more than 10% above the SSC 20 TeV operating current of 6618 A, at the start of testing before achieving a plateau of conductor-limited quenches. Subsequent plateaus at two thermal cycles were re-established without any more training quenches. Mean plateau current was 7407 A, about 0.5% lower than the value of 7442 A predicted from short sample cable measurements. The three plateaus were at slightly different mean values due to slight differences in the test temperature between thermal cycles. All plateau quenches were conductor-limited and occurred in the straight sections of the pole turns, as is expected. The conductor-limited quench plateau was achieved in DSA207 with the standard test ramp rate of 16 A/s.

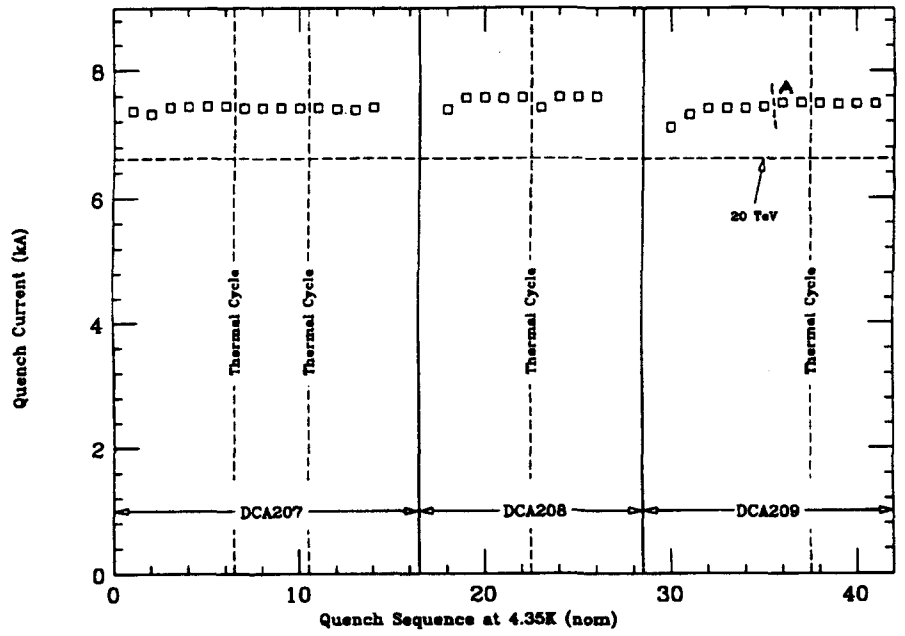


**Figure 11.** BNL-Built 50 mm, 15 m SSC Dipole Quench Tests at 4.35K

During the second cycle of tests for DCA207, quench studies were also done at the lower temperatures of 3.85 K and 3.5 K, after the second plateau at 4.35 K had been established, as mentioned above. In both temperature regimes, the magnet achieved a plateau without any training quenches. At 3.85 K, the plateau mean current was 8073 A, 0.3% above the short sample prediction of 8047 A; at 3.5 K, the plateau mean current was 8422 A, 0.1% below prediction. All quenches were in the lower inner coil ramp-splice section, a region of high field.

From Figure 11, it is also seen that DSA208 was just as well-behaved. There was one training quench at 7383 A before achieving a conductor-limited plateau; after a thermal cycle warmup and re-cooling, the magnet once again established a plateau with one training quench, this time at 7407 A. Both training quenches were about 12% above the SSC 20 TeV operating point. The plateau mean was 7571 A, 0.6% above the short sample prediction of 7524 A, and all plateau quenches were located in the upper inner coil pole turn left straight section. The ramp rate used to achieve the plateau in this magnet was 4 A/s. At the 16 A/s ramp rate, the quench plateau was uniform but about 100 A lower in current and in a turn further in toward the midplane. Again, due to cryogenic test temperature differences between thermal cycles, the two plateaus were at slightly different mean currents.

At 4 A/s, after two training quenches, DCA209 reached a plateau of 7405 A, 1.4% below the short sample prediction of 7508 A and not conductor-limited, as evidenced by

its non-pole turn location. It was found that at 1 A/s, (point A), the magnet exhibited a conductor-limited plateau at 7488 A, 0.3% below the short sample value and located in the same cable region as in DSA208. The lowest training quench was 7102 A, 7% above the 20 TeV operating point of 6618 A. Due to differences in the conductor characteristics among the three magnets, the maximum ramp rate at which a conductor-limited quench plateau could be established was different for all three magnets. In general, at higher ramp rates, heating due to eddy currents generated in loops between the wires in the cable result in quenches located in cable turns further in toward the midplane rather than in a pole turn and also, because of lower field strength, in lower quench currents. It is suspected that a lowering of inter-strand resistance during the coil curing process may be the cause of this effect, and it is presently under investigation. The ramp-dependent behavior of all three magnets was studied by performing a series of quench tests at increasing ramp rates up to 300 A/s for each magnet. The results are shown in Figure 12. Each magnet shows a significantly different behavior, both by the way quench current varies with the ramp rate and by the maximum value at which a conductor-limited quench plateau is achievable. DCA209 showed the unexpected behavior at a noticeable ramp rate dependence in going from 4 A/s to 1 A/s as shown in Figure 12, point A. It is interesting to note that for this cable, the ramp rate dependence is less severe at high ramp rates than at the low one. Studies of this effect are continuing.

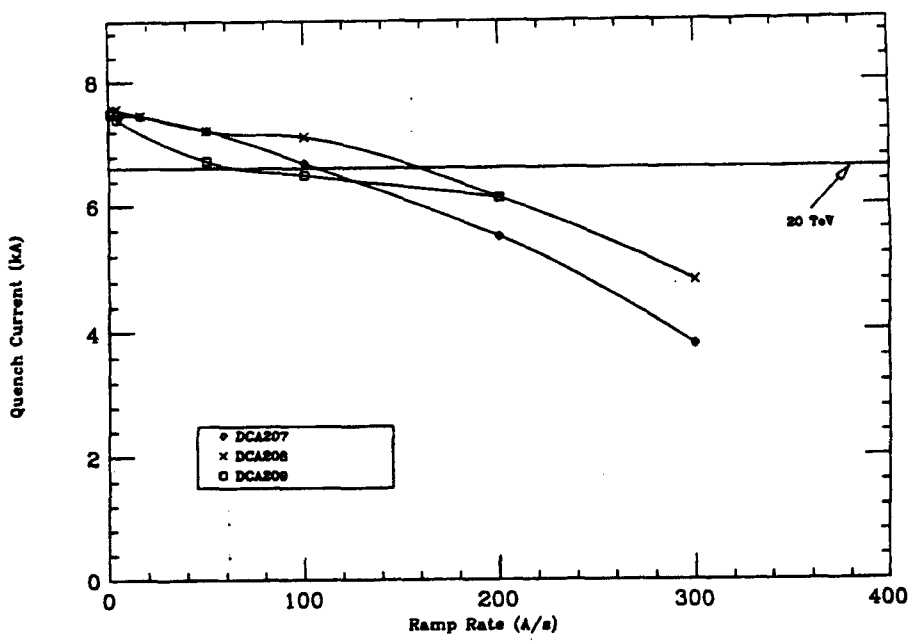


**Figure 12.** 15 m, 50 mm SSC Dipole Magnet Ramp Rate Studies at 4.35 K.

## REFERENCES


[1] J. Kuzminski, et al., "Test results of BNL built 40-mm aperture, 17 m-long SSC Collider dipole magnets", IEEE Trans. Magnetics 28, p.311 (1992).

[2] P. Wanderer, "A Summary of SSC dipole magnet field quality measurements", paper to this conference (Fourth Annual International Industrial Symposium on the Super Collider, New Orleans, LA, March, 1992).

[3] R.C. Gupta, et al., "SSC 50 mm Dipole Cross Section", Supercollider 3, p.387, Plenum Press, NY 1991.

[4] R.P. Shutt and M.L. Rehak, "Transverse Cooling in SSC Magnets", Supercollider 2, p.209, Plenum Press, NY 1990.

# QUENCH PERFORMANCE OF SIX SIMILAR 17 m-LONG, 40 mm-APERTURE SSC MODEL DIPOLES*

P. Wanderer and E. Willen

Accelerator Development Department
Magnet Division
Brookhaven National Laboratory
Upton, New York 11973

## SUMMARY

The quench performance of the final six 17 m-long, 40 mm-aperture SSC model dipoles made at Brookhaven National Laboratory is presented in summary form. The six magnets are of similar construction, except for two features: (1) the copper-to-superconductor ratio of the inner cable (either 1.3:1 or 1.5:1) and (2) the axial preload at 4.35K. The inner coil quench performance does not appear to be correlated with the copper-to-superconductor ratio. There does appear to be a correlation between the outer coil quench performance and the cold axial preload.

## INTRODUCTION

The construction of the final six full-length 40 mm-aperture Collider dipoles at BNL was intended, among other things, to test the effect of the inner coil copper-to-superconductor ratio on quench performance. The first three magnets, DC0201 - DC0203, had Cu:S.C. = 1.5:1 and the last three, DC0204 - DC0206, had Cu:S.C. = 1.3:1. The stability of cable in short-sample measurements has been found to be dependent on the Cu:SC ratio.[1] In other respects the magnets were intended to be alike, with axial and azimuthal preload in operation up to 6.5 kA (6.6 T). Construction details pertinent to this note are listed in Table I. The remaining construction features are described more fully elsewhere[2,3].

First, this note examines the quench performance of the inner coils. The quench performance of the magnets is shown in Figs. 1 - 6. All of the magnets achieved a plateau at 4.35 K, with the plateau quenches originating in the inner coil. Four of the magnets quenched repeatedly in the pole turn (turn 16), indicating conductor limited quenches. For these magnets, the ratio of the conductor limited quench current, $I_{CL}$, to the quench current

*This work supported by the U.S. Department of Energy.

estimated from short-sample tests, $I_{SS}$, is tallied in Table II. In two of the magnets, the plateau quenches originated in turns near the pole turn as noted in Table II. For these magnets, the data yield only a limit on the ratio $I_{CL}/I_{SS}$. The limit is probably 1% - 2% below the actual value of the ratio. This uncertainly limits the accuracy of the comparison to about 2%, which is comparable to the uncertainty from other sources such as magnet temperature and short-sample measurements. (The three magnets made with Cu:S.C. = 1.3:1 all contain cable from the same spool; $I_{CL}/I_{SS}$ varies 1% in this set.) Within this 2% uncertainty, $I_{CL}/I_{SS}$ shows no dependence on the Cu:S.C. ratio.

Another approach to testing for effects of the Cu:S.C. ratio is to count the number of inner coil training quenches. This enumeration can be broken into three parts: initial quenching, quenching after a thermal cycle, and quenching at low tempeerature. (Outer coil quenches have been ignored for this exercise.) In the initial quench testing, one of the three magnets in each group has no training quenches and the other two do. The total number of training quenches for each group of three magnets (two for the magnets with Cu:S.C. = 1.5:1, four for the magnets with Cu:S.C. = 1.3:1) is small and not significantly different for the two groups. After the thermal cycle, the two groups have the same performance (one magnet with no retraining, two magnets with one retraining quench each). At low temperature, all three magnets with Cu:S.C. = 1.5:1 reach plateau with little additional training as does the one magnet (DC0206) with Cu:S.C. = 1.3:1 whose low temperature performance was not limited by the outer coil. In all, no significant difference is found between the number of training quenches in the two groups of magnets.

When the magnets were tested, quench origins in the outer coil were found in four of the magents. A careful review of the construction features (Table I) and quench performance (Table II) was made. The experiment with magnet DC0201, where outer coil quenches were observed after the end preload was reduced, coupled with experience with the 1.8 m-long, 50 mm-aperture magnets, which had improved quench performance as a result of increasing the end preload,[4] suggested that increasing the end preload might help. Consequently, the room temperature end preload in the last magnet, DC0206, was increased significantly. No quenches occurred in the outer coils of this magnet. A review of the outer coil quenches and end loading of these magnets shows a simple correlation: magnets with end preload at 4.35 K of 5600 lbs. or more do not quench in the outer coil; those with cold end preload of 2000 lbs. or less do.[5]

In addition to the warm end preload, two factors influenced the cold end preload. First, the interface between the yoke and collars was changed due to the addition of 3 mil shims after magnet DC0201. Second, the yoke packing factor was increased for the last four magnets. The combination of these two changes clearly influenced the axial preload during cooldown. The DC0201 end preload increased 5600 lbs. during cooldown, whereas the largest increase in the later magnets was 200 lbs., and most lost significantly. The large increase in the warm end preload of DC0206 compensated for the observed cooldown loss in the magnets with yoke-collar shims and extra laminations.

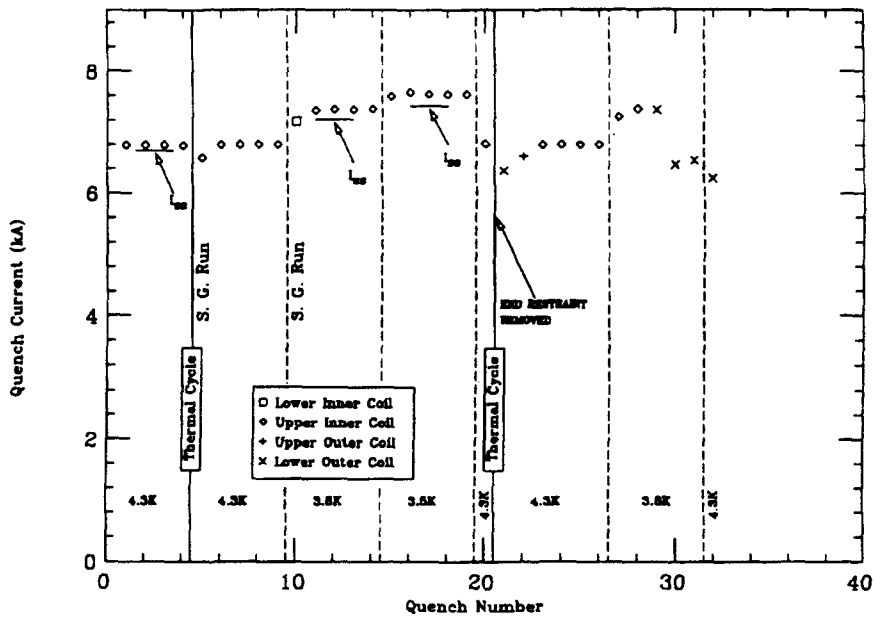


**Figure 1.** **Quench history for magnet DC0201. This magnet was conditioned by ramping three times to 6.8 kA at 3.5 K before the first quench.**

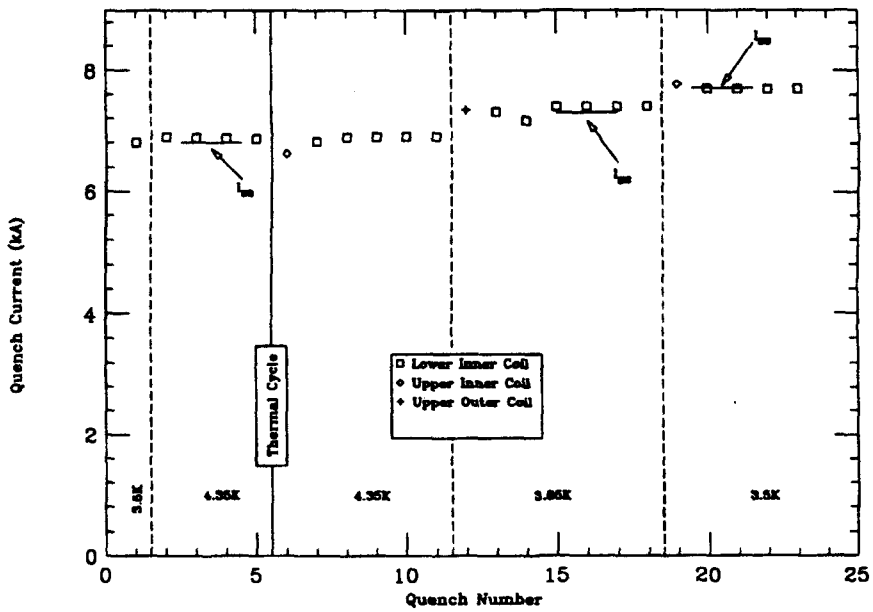


**Figure 2. Quench history for magnet DC0202**

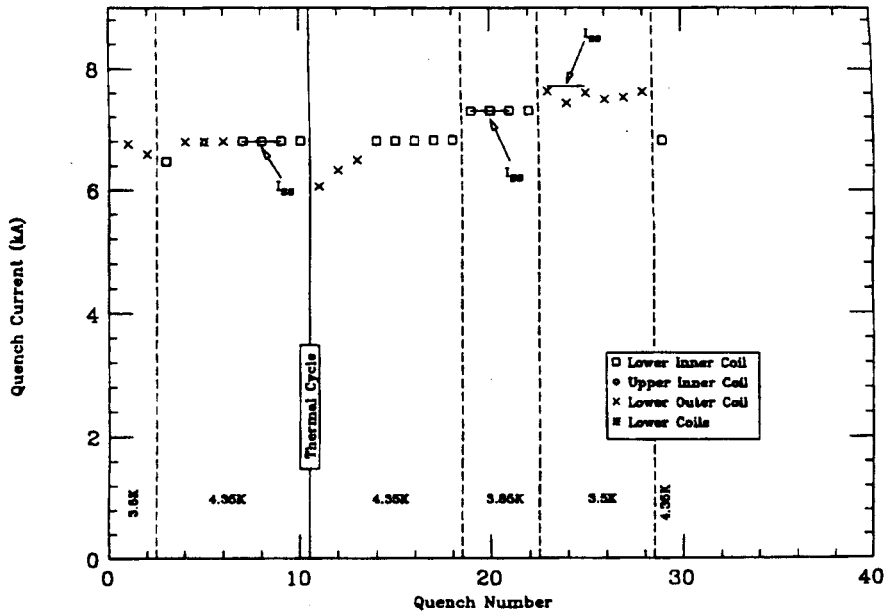


**Figure 3. Quench history for magnet DC0203.**

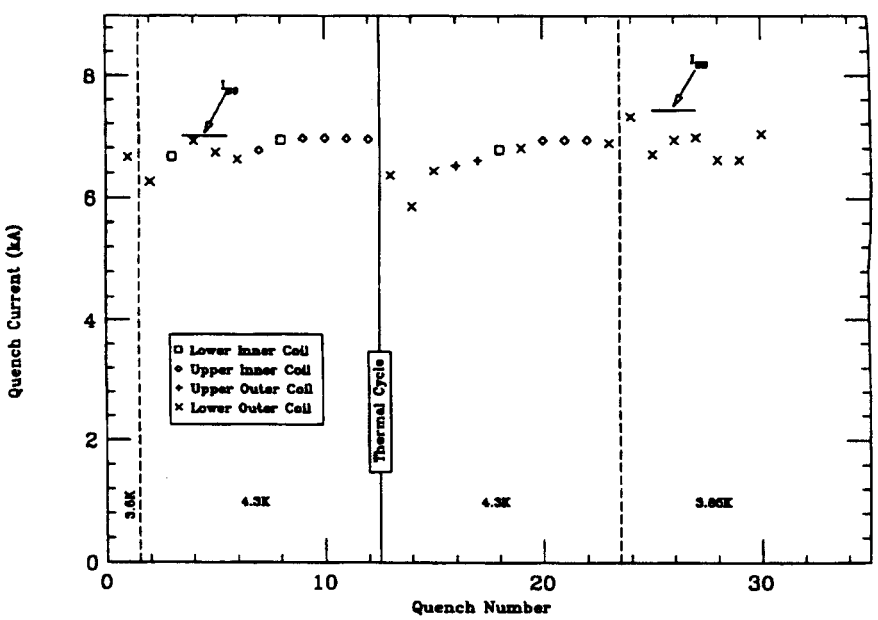


**Figure 4. Quench history for magnet DC0204.**

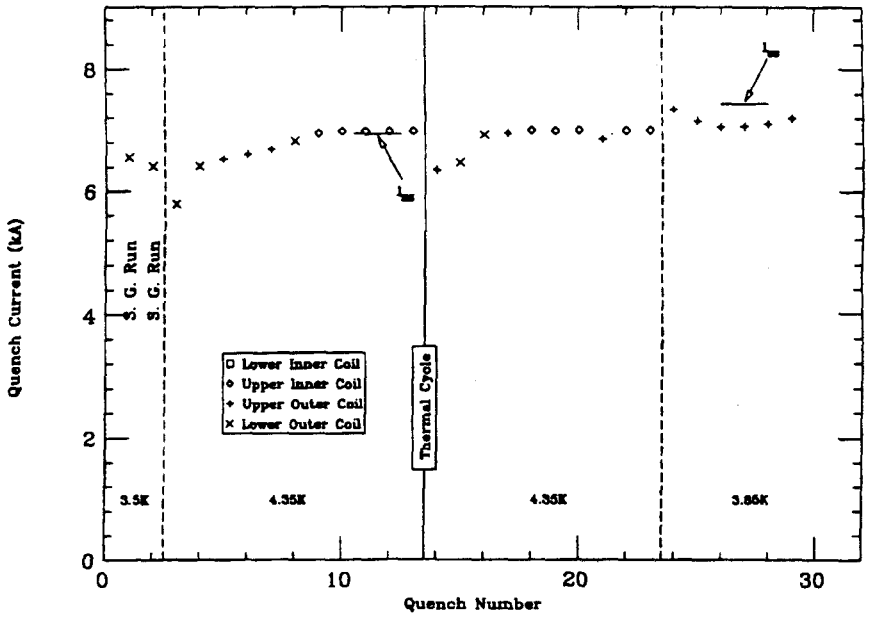


Figure 5. Quech history for magnet DC0205.

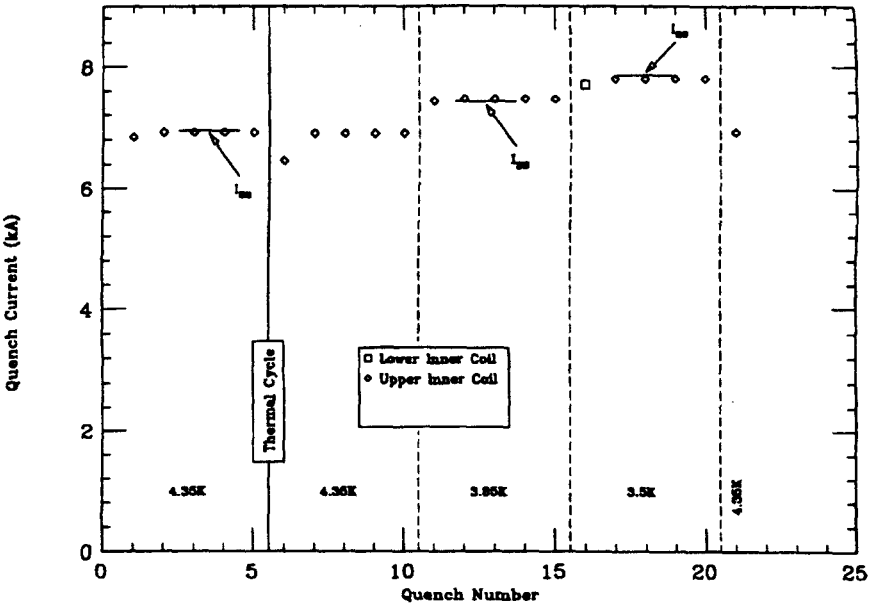


Figure 6. Quench history for magnet DC0206. This magnet was conditioned by ramping three times to 6.8 kA at 3.5 K before the first quench.

**Table I.** Magnet Construction Features

| Magnet | Cable Inner | Cable Outer | $I_C$(7T) | $I_{SS}$(A) 4.35K | Cable FG Epoxy Content (%) I | Cable FG Epoxy Content (%) O | Cu:SC Inner | Yoke Weight (lbs.) Before extra Lams. | Yoke Weight (lbs.) After extra Lams. | No. of Laminations Added |
|---|---|---|---|---|---|---|---|---|---|---|
| DC0201 | I-B0310 | S-2071 | 7851 | 6738 | 24 | 24 | 1.5:1 | 11295.06 | 11295.06 | 0 |
| DC0202 | I-5264 | I-B0359 | 7791 | 6800 | 20 | 24 | 1.5:1 | 11306.20 | 11306.20 | 0 |
| DC0203 | I-5264 | I-B0359 | 7791 | 6800 | 20 | 24 | 1.5:1 | 11306.76 | 11315.36 | 7 |
| DC0204 | S-2346 | I-B0397 | 8368 | 6944 | 20 | 24 | 1.3:1 | 11307.64 | 11315.24 | 7 |
| DC0205 | S-2346 | I-B0359<br>I-B0397 | 8368 | 6944 | 20 | 24 | 1.3:1 | 11309.29 | 11321.19 | 11 |
| DC0206 | S-2346 | I-B0640<br>I-B0641 | 8368 | 6944 | 20 | 20 | 1.3:1 | 11309.39 | 11314.79 | 5 |

NOTES:

1. 201: No shims; 202-206: 3 mil shims at poles between collar and yoke.
2. 202, 203, 205, 206: Increased end force before test.
3. 203: Asymmetry of one outer coil wedge reversed.
4. 201, 204: Bridge, via RTV/weld of end tubes, between end plate and yoke.
5. This series of magnets used low carbon steel spacers between blocks rather than stainless steel spacers as used in earlier magnets.
6. The yoke design specified a fixed weight of steel over the specified yoke length. When spaces between yoke blocks developed because of more compact yoke blocks, extra laminations were mistakenly added in the later magnets, giving a higher yoke density in these magnets.

**Table II.** Magnet Performance.

| Magnet | Cold Azimuthal Prestress $\sigma$,Inner, I=0 (PSI) | Cold Azimuthal Prestress $\sigma$,Outer, I=0 (PSI) | Cold Azimuthal Prestress $I^2$ for $\sigma$,Inner=0 $(kA)^2$ | Total End Force (lbs.) After Welding | Total End Force (lbs.) Cold, Before Q | Total End Force (lbs.) Cold, After Q | Total End Force (lbs.) Force at $I^2=40(kA)^2$ | No. of Training Q I | No. of Training Q O | $I_{CL}$(A) | $I_{CL}/I_{SS}$ |
|---|---|---|---|---|---|---|---|---|---|---|---|
| DC0201 | 4000 | 3800 | 27 | 1400 | 5600 | 7200 | 9000 | 0 | 0 | 6788 | 1.007 |
| DC0202 | 3220 | 2970 | 28 | 3100 | 1600 | 4130 | 6800 | 1 | 0 | >6899 | >1.015 |
| DC0203 | 2340 | 4130 | 22 | 3690 | 1910 | 3060 | 5600 | 1 | 5 | >6803 | >1.000 |
| DC0204 | 3000 | 3800 | 25 | 1600 | 1800 | 3600 | 6000 | 3 | 5 | 6961 | 1.002 |
| DC0206 | 2820 | 3900 | 25 | 2800 | 2000 | 2800 | 4000 | 0 | 8 | 6985 | 1.006 |
| DC0206 | 5200 | 4400 | 31 | 10000 | 6000 | 7400 | 10700 | 1 | 0 | 6920 | 0.997 |

NOTES:

1. 202: $I_{CL}$ from the second quench. The other plateau quenches originated in turn 13.
2. 203: All plateau quenches originated in turn 15.
3. The outer coil quenching observed in the training of some of the magnets persists also in the lower temperature quenching tests of these magnets.
4. The fourth column indicates the value of $I^2$ beyond which the inner coil prestress is zero. For I = 6.5 kA, $I^2$ = 42 $(kA)^2$.

## REFERENCES


1. A.K. Ghosh, M. Garber, K.E. Robins and W.B. Sampson, "Training in Test Samples of Superconducting Cables for Accelerator Magnets," IEEE Trans. Magnetics 25:1831 (1989).

2. J. Kuzminski et al., "Test Results of BNL Built 40 mm-Aperture, 17 m-Long SSC Collider Dipole Magnets," IEEE Trans. Magnetics 28:311 (1992).

3. A. Devred et al., About the Mechanics of SSC Dipole Magnet Prototypes, in: "The Physics of Particle Accelerators," American Institute of Physics, NY (1992).

4. J.F. Muratore et al., "Construction and Test Results from 1.8 m-Long, 50 mm Aperture SSC Model Collider Dipoles," paper to this conference (IISSC 92).

5. The outer coil quenches in DC0203 may not bear on the question of axial restraint, since all but three were near the location of the incorrectly-installed outer coil wedge (see Table I). The three quenches after the thermal cycle were far from this wedge. But the last two of these occurred near the warm end of the magnet when the temperature rise across the magnet was unusually high (100 mk versus 40 mk).

# QUENCH PLATEAU, COIL CURE TEMPERATURE, AND COPPER-TO SUPERCONDUCTOR RATIO IN RECENT 1.8 m SSC MODEL DIPOLES*

P. Wanderer

Accelerator Development Department
Magnet Division
Brookhaven National Laboratory
Upton, New York 11973

## SUMMARY

The ratio of the conductor-limited quench currents to the short-sample prediction, $I_Q/I_{SS}$, is tabulated for a series of 1.8 m-long SSC model collider dipoles. Sixteen of these magnets have 40 mm aperture, four have 50 mm aperture. For these magnets, the coil cure temperature ranged from 135 C to 217 C and the ratio of copper-to-superconductor ranged from 1.27 to 1.54. At 4.35 K, the value of $I_Q/I_{SS}$ was between 1.00 and 1.04 with no clear dependence on cure temperature or Cu:S.C. ratio.

**********

This note collects data from recent short SSC R&D dipoles made at BNL. All the magnets reached a stable quench plateau at a nominal temperature of 4.35 K, as summarized in Table I. In all the magnets, these conductor limited quenches occurred in the pole turn of the inner coil, as expected. The magnet plateau current is compared to the expected value $I_{SS}$, which has been calculated from the 7 T value of the critical current $I_C$ using G. Morgan's parameterization (AUTOIC90).

The Table also lists two construction features: the copper-to-superconductor ratio of the cable used in the inner coil and the cure temperature of the coils during molding. The cure temperatures are dictated by the choice of cable insulation. For the DSS magnets and DSA207, 208 in the Table, the standard epoxy-fiberglass-Kapton scheme was used. For the DS020n magnets, different combinations of all-Kapton insulation were used. The polyimide adhesive used in DS0201-DS0204 required a higher cure temperature than the epoxy used in DS0205, 206. DSA209, 210 also had polyimide adhesive.

---

*This work is supported by the U.S. Department of Energy

Generally speaking, the uncertainties in the ratio $I_Q/I_{SS}$ are estimated to be at the level of 2%. This includes uncertainties in both $I_C$ (7 T) and $I_Q$ and possible vendor-to-vendor differences (e.g., IGC SI-64 vs. OST SC14-2).[1] Within this uncertainty, the plateau current as a fraction of short sample does not appear to be affected by the different cure cycles or copper-to-superconductor used in these magnets.

**Table I.** Quench Plateau and Construction Data for 1.8 m long, 40 mm and 50 mm Aperture SSC Dipoles

| 40 mm Aperture Magnets | Nominal Coil Cure Temp. (C) | Cable for Inner Coils | Cu:SC Ratio | $I_C$ (7 T) (A) | $I_{SS}$ (A) (4.35 K) | $I_Q$ (A) | $I_Q/I_{SS}$ |
|---|---|---|---|---|---|---|---|
| DSS013 | 135 | IGC SI-64 | 1.47 | 7741 | 6784 | 6950 | 1.024 |
| DSS014 | 135 | IGC SI-64 | 1.47 | 7741 | 6784 | 6855 | 1.010 |
| DSS016 | 135 | IGC SI-64 | 1.47 | 7741 | 6784 | 6950 | 1.024 |
| DSS017 | 135 | IGC SI-64 | 1.47 | 7741 | 6784 | 6925 | 1.020 |
| DSS018 | 135 | OST SC14-2 | 1.53 | 7020 | 6577 | 6790 | 1.032 |
| DSS019 | 135 | OST SC14-2 | 1.53 | 7020 | 6577 | 6770 | 1.029 |
| DSS020 | 135 | OST SC14-2 | 1.53 | 7020 | 6577 | 6810 | 1.035 |
| DSS021 | 135 | OST SC14-2 | 1.53 | 7020 | 6577 | 6820 | 1.037 |
| DS0201 | 217 | IGC SC13-3 | 1.53 | 7851 | 6803 | 6875 | 1.009 |
| DS0202 | 217 | IGC SC13-3 | 1.53 | 7851 | 6803 | 6865 | 1.007 |
| DS0203 | 217 | IGC SC13-3 | 1.53 | 7851 | 6803 | 6895 | 1.012 |
| DS0204 | 217 | OST (SSC-I-0-11) | 1.27 | 8603 | 6997 | 7060 | 1.009 |
| DS0205 | 170 | OST (SSC-I-0-11) | 1.27 | 8603 | 6997 | 7040 | 1.006 |
| DS0206 | 170 | OST (SSC-I-0-11) | 1.27 | 8603 | 6997 | 7060 | 1.009 |
| DS0213 | 217 | OST (SSC-I-0-11) | 1.27 | 8603 | 6997 | 7015 | 1.003 |
| DS0214 | 217 | OST (SSC-I-0-11) | 1.27 | 8603 | 6997 | 7036 | 1.006 |
| **50 mm Aperture Magnets** | **Nominal Coil Cure Temp. (C)** | **Cable for Inner Coils** | **Cu:SC Ratio** | **$I_C$ (7 T) (A)** | **$I_{SS}$ (A) (4.35 K)** | **$I_Q$ (A)** | **$I_Q/I_{SS}$** |
| DSA207 | 135 | SSC-3-I-22 | 1.54 | 10827 | 7440 | 7500 | 1.008 |
| DSA208 | 135 | SSC-3-I-22 | 1.54 | 10827 | 7440 | 7600 | 1.022 |
| DSA209 | 217 | SSC-3-S-22 | 1.51 | 10079 | 7315 | 7390 | 1.010 |
| DSA210 | 217 | SSC-3-S-22 | 1.51 | 10079 | 7315 | 7405 | 1.012 |

[1]For cable SC13-3, $I_{SS}$ is the average of measurements made on four different segments covering 80% of the cable length which have an rms variation of 20 A. $I_C$ data from one end of the cable were about 1-1/2% lower and were not used in the average. The magnets reported here used cable from the opposite end of the spool. For DS0203, $I_{SS}$ is for the coil half in which the plateau quenches occurred.